frontiers | Frontiers in Physics

TYPE Original Research
PUBLISHED 03 November 2025
DOI 10.3389/fphy.2025.1657967

OPEN ACCESS

EDITED BY
Ryosuke Yano,
Tokio Marine dR Co., Ltd., Japan

REVIEWED BY
Abdellatif Ben Makhlouf,
University of Sfax, Tunisia
Norikazu Saito,
The University of Tokyo, Komaba, Japan

*CORRESPONDENCE
Yoichi Enatsu,
yenatsu@rs.tus.ac.jp

RECEIVED 02 July 2025
ACCEPTED 19 September 2025
PUBLISHED 03 November 2025

CITATION
Zeng P, Enatsu Y and Zhou G (2025) A nonlocal advection system for two competing species with resources recovering time. *Front. Phys.* 13:1657967. doi: 10.3389/fphy.2025.1657967

A nonlocal advection system for two competing species with resources recovering time

Ping Zeng[1], Yoichi Enatsu[2]* and Guanyu Zhou[1]

[1]Institute of Fundamental and Frontier Sciences, University of Electronic Science and Technology of China, Chengdu, China, [2]Institute of Arts and Sciences, Oshamambe Division, Tokyo University of Science, Oshamambe, Hokkaido, Japan

Competitive interactions between multiple cell populations are crucial for modeling biological processes such as tumor growth and tissue regeneration. In this study, we investigate the nonlocal advection model for two-species competition, which characterizes cell growth and dispersion phenomena in co-culture experiments. To capture realistic phenomena in biology, we introduce the time delay representing population migration and resources recovering time. The primary objectives are to investigate the impact of time delays on competitive dynamics under various parameter settings and to develop numerical methods that ensure biological feasibility of solutions. Accordingly, we design a positivity-preserving finite volume scheme based on an upwind flux approach, guaranteeing non-negative population densities and discrete conservation properties. We examine the convergence orders of the scheme through the numerical experiments and explore the effects of time delays on species competition dynamics under different parameter settings.

KEYWORDS

two species model, time delay, hyperbolic PDE, Keller–Segel model, advection, nonlocal

1 Introduction

The mathematical modeling of multi-species population dynamics provides a theoretical framework for studying species interactions in biological and ecological systems [1, 2]. In biochemical research, scientists employ co-culture systems to elucidate competitive relationships between distinct cell types, such as cancer cells and normal cells [3]. Early models included nonlinear diffusion and reaction-diffusion systems [4, 5, 6], revealing that spatial segregation can promote species coexistence by mitigating interspecific competition. A key approach in modern models involves nonlocal advection systems [7, 8], where population movement is influenced by long-range interactions instead of purely local diffusion. These models are often associated with chemotaxis, the directed movement of cells or organisms along chemical concentration gradients [9, 10, 11, 12]. The well-posedness of nonlocal advection models for two species (or a single species) has been studied in [7, 8, 13, 14]. Moreover, nonlocal advection systems are closely connected to continuum models of pedestrian dynamics, where an individual's velocity is influenced not only by local density but also by spatially distributed crowd information [15, 16]. Extensions considering anisotropic interactions and domain boundaries further demonstrate the relevance of nonlocal frameworks to realistic crowd flow modeling [17, 18].

Time delays capture the inherent non-instantaneous nature of biological processes, yielding more realistic models that can exhibit oscillatory, bifurcation, and stability

behaviors observed in real systems [19, 20]. Following the pioneering work of [21], numerous studies have introduced time delays in population dynamics models. In single species models such as the delayed logistic model [22, 23, 24], the delay represents the maturation time before individuals become reproductively active and can destabilize population dynamics by inducing oscillations or periodic behavior once it exceeds a critical threshold. The time delayed Lotka–Volterra predator-prey model [25, 23, 26] incorporates the predator's delayed response to changes in prey population, enabling more accurate simulations of periodic oscillations and stability shifts in ecosystems. Time lags in competition models [27, 28] physically represent ecological processes such as resource recovery or interspecific interaction lags, and they can destabilize equilibrium states to induce stable periodic oscillations or even chaotic dynamics through Hopf bifurcation or period-doubling bifurcations.

This study aims to extend the existing nonlocal advection model for two competing species by incorporating time delays. Previous studies focused on population mobility and interactions, while our study introduces time delays to characterize the interaction between population migration and resource recovery. To ensure biologically realistic population densities, we develop a positivity-preserving finite volume scheme. We conduct extensive numerical experiments to: (1) examine the numerical convergence orders; (2) investigate the influence of time delays on competitive dynamics under various parameter settings.

In this work, we first introduce the mathematical model—the two species hyperbolic Keller–Segel system with time delays, and then design a finite volume scheme satisfying the positivity-preserving property, where we adopt the upwind type flux similar to [29–32, 33]. We investigate the experimental convergence orders of the proposed scheme. According to the numerical simulation, under various parameter settings, we find that small, identical delays in both species lead to a steady state, whereas larger delays may induce unsteady and potentially the extinction of one or both species. Moreover, asymmetric delay parameters between the two species tend to confer a competitive advantage to one species.

The rest of this paper is organized as follows. In Section 2, we extend the nonlocal advection Keller–Segel model by incorporating time delay and develop a positivity-preserving finite volume method that also satisfies discrete conservation laws. Numerical examples are presented in Section 3.

2 The mathematical model and the finite volume scheme

In this section, we introduce the time delay to the classical hyperbolic Keller–Segel system and design a positivity-preserving finite volume scheme.

2.1 PDE model

We consider the nonlocal advection system for two competing species with time delays in an interval $I = [a, b]$. We denote by $u_j(t,x)$ $(j = 1,2)$ the density of two species. The PDE model is stated as follows.

$$\partial_t u_1 - d_1 \partial_x \left(u_1 \partial_x p\right) = u_1 h_{1,\alpha_1}(u_1, u_2) \quad \text{in } (0,T]\times I, \tag{2.1a}$$

$$\partial_t u_2 - d_2 \partial_x \left(u_2 \partial_x p\right) = u_2 h_{2,\alpha_2}(u_1, u_2) \quad \text{in } (0,T]\times I, \tag{2.1b}$$

$$\left(I - \chi\Delta\right) p = u_1 + u_2 \quad \text{in } (0,T]\times I, \tag{2.1c}$$

$$\partial_x p(t,a) = \partial_x p(t,b) = 0 \quad \text{on } (0,T], \tag{2.1d}$$

$$u_1(t,x) = u_{1,0}(x) \quad \text{in} \quad I,\ t \le 0, \tag{2.1e}$$

$$u_2(t,x) = u_{2,0}(x) \quad \text{in} \quad I,\ t \le 0, \tag{2.1f}$$

where ν is the outward normal vector, d_j $(j = 1,2)$ is the dispersion coefficient, χ is the sensing coefficient. The function $p(t,x)$, which represents the pressure or chemical potential field induced by species densities, satisfies the elliptic Equations 2.1c, 2.1d, and its gradient $\partial_x p$ influences the movement direction of the species u_j $(j = 1,2)$. We set, for $\alpha_1, \alpha_2 \ge 0$,

$$h_{1,\alpha_1}((u_1,u_2)(t,x)) = b_1 - \delta_1 - \left(a_{11}u_1(t-\alpha_1,x) + a_{12}u_2(t,x)\right), \tag{2.2a}$$

$$h_{2,\alpha_2}((u_1,u_2)(t,x)) = b_2 - \delta_2 - \left(a_{21}u_1(t,x) + a_{22}u_2(t-\alpha_2,x)\right), \tag{2.2b}$$

where $b_j > 0$ $(j = 1,2)$ are the growth rates, $a_{jj} \ge 0$ $(j = 1,2)$ represent the intraspecific competition coefficients, reflecting competition between individuals of the same species, $a_{12}, a_{21} \ge 0$ denote the interspecific competition coefficients between species, $\alpha_j \ge 0$ $(j = 1,2)$ represent the delay parameters, and δ_j $(j = 1,2)$ are the additional mortality rates caused by drug treatment. The delay parameters α_j in h_{j,α_j} $(j = 1,2)$ represent time lags in intraspecific competition of species u_j $(j = 1,2)$, reflecting delayed self-density feedback from migration and resource recovery. When $\alpha_1 = \alpha_2 = 0$, Equations 2.1a–2.1f is the hyperbolic Keller–Segel system proposed in [14].

2.2 The finite volume scheme

We introduce the fully discrete finite volume scheme for problem Equations 2.1a–2.1f. We hereafter denote by $|\omega|$ the measure of the interval ω in $\mathbb{R}$.

2.2.1 The finite volume scheme

For simplicity, we divide the computational domain $I = [a,b]$ into N_c cells (see Figure 1):

$$C_i = \left\{x:\ x_{i-\frac{1}{2}} \le x \le x_{i+\frac{1}{2}}\right\}, \quad 1 \le i \le N_c,$$

where

$$a = x_{\frac{1}{2}} < x_{\frac{3}{2}} < \cdots < x_{N_c+\frac{1}{2}} = b.$$

We denote by $x_i = (x_{i+\frac{1}{2}} + x_{i-\frac{1}{2}})/2$ the center of the cell C_i, and set

$$h_i = x_{i+\frac{1}{2}} - x_{i-\frac{1}{2}} \quad \left(1 \le i \le N_c\right), \qquad h = \max_{1\le i\le N_c} h_i.$$

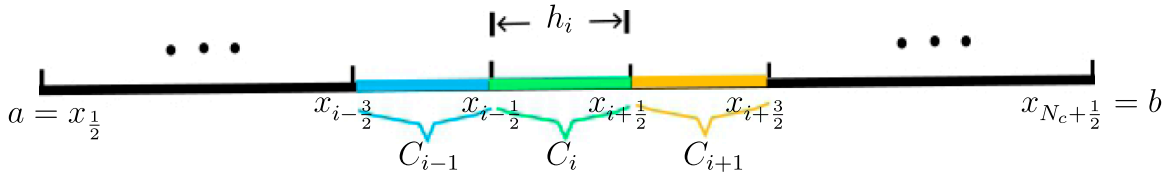

FIGURE 1
The mesh for the interval I.

TABLE 1 Experimental errors and convergence order of h for $\alpha_1 = \alpha_2 = 0$ (Example 1-1).

h	$\|u^N_{1,ref} - u^N_{1,h}\|_{L^2(I),\mathcal{V}_h}$	rate	$\|u^N_{2,ref} - u^N_{2,h}\|_{L^2(I),\mathcal{V}_h}$	rate	$\|p^N_{ref} - p^N_h\|_{H^1(I),\mathcal{V}_h}$	rate
1/80	1.29E-01	-	3.02E-02	-	1.11E-02	-
1/160	8.23E-02	0.64	1.78E-02	0.76	5.90E-03	0.90
1/320	4.81E-02	0.78	9.80E-03	0.86	3.00E-03	1.01
1/640	2.38E-02	1.01	4.70E-03	1.07	1.30E-03	1.21

TABLE 2 Experimental errors and convergence order of h for $\alpha_1 = \alpha_2 = 0.5$ (Example 1-2-2).

h	$\|u^N_{1,ref} - u^N_{1,h}\|_{L^2(I),\mathcal{V}_h}$	rate	$\|u^N_{2,ref} - u^N_{2,h}\|_{L^2(I),\mathcal{V}_h}$	rate	$\|p^N_{ref} - p^N_h\|_{H^1(I),\mathcal{V}_h}$	rate
1/80	1.35E-01	-	3.25E-02	-	1.20E-02	-
1/160	8.55E-02	0.66	1.89E-02	0.78	6.40E-03	0.90
1/320	4.95E-02	0.79	1.03E-02	0.88	3.20E-03	1.02
1/640	2.43E-02	1.03	4.80E-03	1.08	1.40E-03	1.22

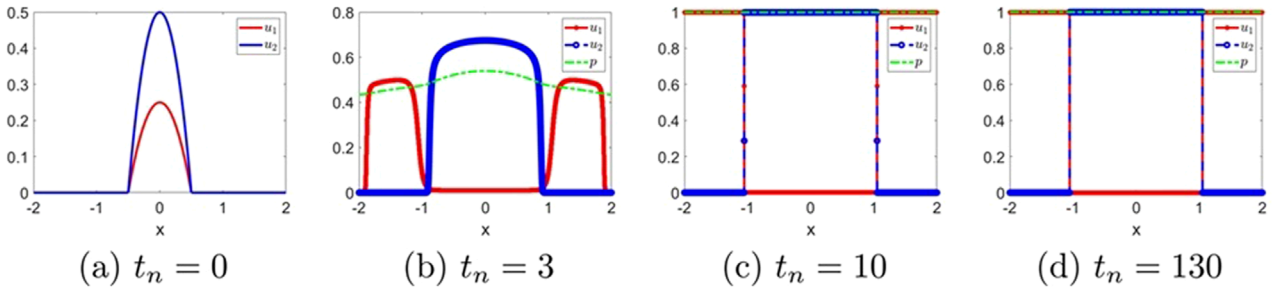

FIGURE 2
The numerical solution for $\alpha_1 = \alpha_2 = 0$ (Example 1-1). **(a–d)** show the evaluation of the numerical solution at different times.

We introduce the space of the piecewise constant function:

$$\mathcal{V}_h = \left\{ v_h \in L^\infty(I) : v_h|_{C_i} \in P_0(C_i) \quad \text{for all } C_i \right\},$$

where $P_0(C_i)$ represents the set of constant functions in cell C_i.

We assume that there are two integers M_1 and M_2 such that the delay parameters satisfy $\alpha_2 = (M_2/M_1)\alpha_1$. Let $\tau = \alpha_1/(KM_1)$ for some integer K. We can take the integers $m_1 = KM_1$, $m_2 = KM_2$. Then we see that $\alpha_1 = m_1\tau$, $\alpha_2 = m_2\tau$.

Let N be the smallest integer such that $N\tau \geq T$. The time interval is divided into N segments:

$$0 = t_0 < t_1 < \cdots < t_n < t_{n+1} < \cdots < t_N, \quad \text{with} \quad t_n = n\tau,$$

and we use the backward Euler to approximate time-differential, i.e.,

$$\partial_\tau v^n := \frac{v^n - v^{n-1}}{\tau} \approx v_t(t_n) \quad (v^n = v(t_n)).$$

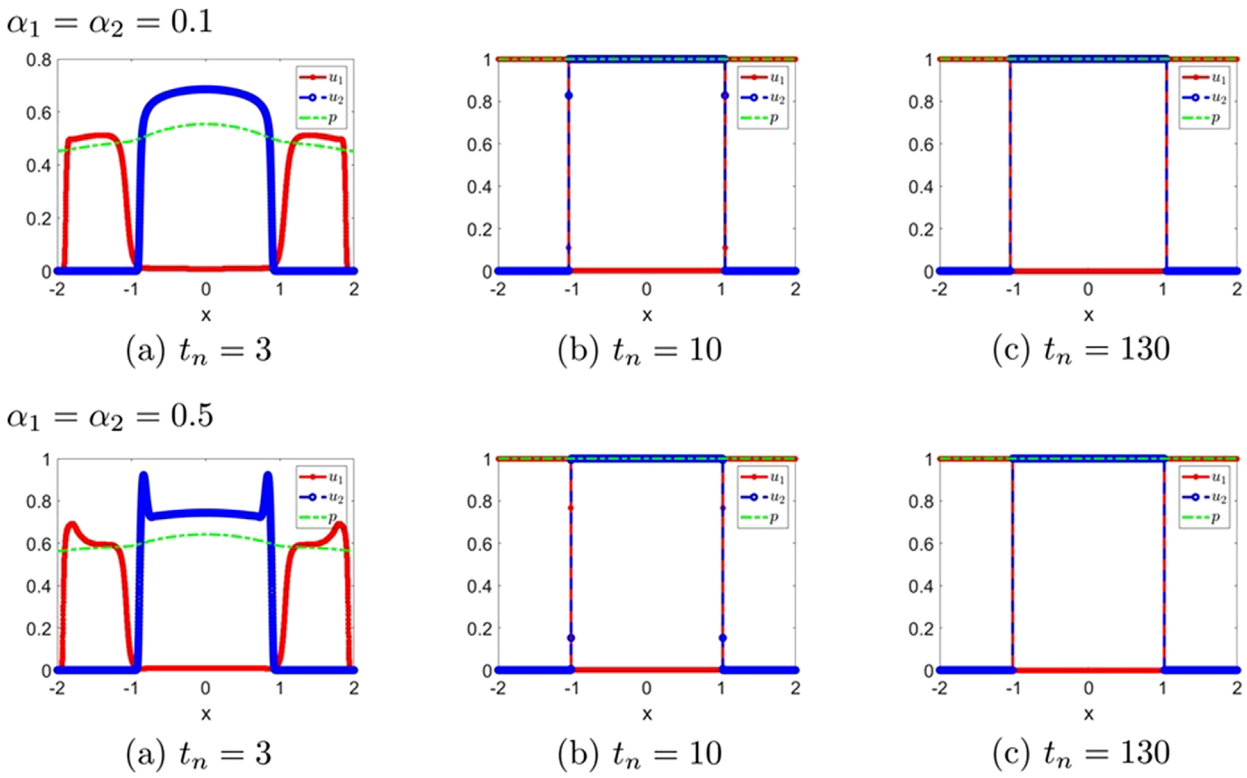

FIGURE 3
The numerical solution (Examples 1-2-1, 1-2-2). **(a–c)** show the evaluation of the numerical solution at different times.

Let $p_h^n, u_{1,h}^n, u_{2,h}^n \in \mathcal{V}_h$ be the numerical approximation to $p(t_n,x), u_1(t_n,x), u_2(t_n,x)$ $(n = 0,1,\ldots,N)$. The proposed scheme is described below.

By integrating Equations 2.1a–2.1c on each cell C_i and applying integration by parts, we obtain the following implicit scheme at $t = t_n$ using the backward Euler method:

$$\int_{C_i} p(t_n,x)\,dx - \left(\chi \partial_x p(t_n,x)\right)\Big|_{x_{i-\frac{1}{2}}}^{x_{i+\frac{1}{2}}} = \int_{C_i} \left(u_1(t_{n-1},x) + u_2(t_{n-1},x)\right) dx,$$

$$\int_{C_i} \partial_t u_1(t_n,x)\,dx - \left(d_1 u_1(t_n,x)\,\partial_x p(t_n,x)\right)\Big|_{x_{i-\frac{1}{2}}}^{x_{i+\frac{1}{2}}} = \int_{C_i} u_1(t_n,x)\, h_{1,\alpha_1}\left((u_1,u_2)(t_{n-1},x)\right) dx,$$

$$\int_{C_i} \partial_t u_2(t_n,x)\,dx - \left(d_2 u_2(t_n,x)\,\partial_x p(t_n,x)\right)\Big|_{x_{i-\frac{1}{2}}}^{x_{i+\frac{1}{2}}} = \int_{C_i} u_2(t_n,x)\, h_{2,\alpha_2}\left((u_1,u_2)(t_{n-1},x)\right) dx.$$

Using $p^n(x) \approx p_h^n(x_i) := p_i^n, u_1^n(x) \approx u_{1,h}^n(x_i) := u_{1,i}^n, u_2^n(x) \approx u_{2,h}^n(x_i) := u_{2,i}^n$ on C_i, we get:

$$\int_{C_i} p(t_n,x)\,dx \approx |C_i| p_i^n, \qquad \partial_x p(t_n,x)\Big|_{x_{i-\frac{1}{2}}}^{x_{i+\frac{1}{2}}} = \partial_x p\left(t_n, x_{i+\frac{1}{2}}\right) - \partial_x p\left(t_n, x_{i-\frac{1}{2}}\right),$$

$$\int_{C_i} \left(u_1(t_{n-1},x) + u_2(t_{n-1},x)\right) dx \approx |C_i|\left(u_{1,i}^{n-1} + u_{2,i}^{n-1}\right),$$

$$\int_{C_i} \partial_t u_j(t_n)\,dx \approx \int_{C_i} \partial_t u_{j,h}^n(x_i)\,dx = |C_i| \partial_t u_{j,i}^n = |C_i| \frac{u_{j,i}^n - u_{j,i}^{n-1}}{\tau} \quad (j = 1,2),$$

$$\int_{C_i} u_j(t_n,x)\, h_{j,\alpha_j}\left((u_1,u_2)(t_{n-1},x)\right) dx \approx |C_i| u_{j,i}^n h_{j,\alpha_j}\left(u_{1,i}^{n-1}, u_{2,i}^{n-1}\right) \quad (j = 1,2).$$

We use the approximation:

$$\mathbf{P}_{i-\frac{1}{2}}^n := \partial_x p\left(t_n, x_{i-\frac{1}{2}}\right) \approx \begin{cases} \dfrac{p_i^n - p_{i-1}^n}{|x_i - x_{i-1}|} & 2 \le i \le N_c, \\ 0 & i \in \{1, N_c+1\} \end{cases} \tag{2.3}$$

(by Equation 2.1d)

We apply the *upwind* discretization to treat the flux: for $j = 1,2$,

$$-\left(d_j u_j(t_n,x)\,\partial_x p(t_n,x)\right)\Big|_{x_{i-\frac{1}{2}}}^{x_{i+\frac{1}{2}}} \approx F_{j,i+\frac{1}{2}}^n - F_{j,i-\frac{1}{2}}^n,$$

$$F_{j,i-\frac{1}{2}}^n := u_{j,i-1}^n \left[-d_j \mathbf{P}_{i-\frac{1}{2}}^n\right]^+ - u_{j,i}^n \left[-d_j \mathbf{P}_{i-\frac{1}{2}}^n\right]^-,$$

where $[r]^+ = \max\{r,0\}$ and $[r]^- = \max\{-r,0\}$. The upwind type numerical flux can be understood as follows. If the "flux" is from C_{i-1} towards C_i (i.e., $-d_j \mathbf{P}_{i-\frac{1}{2}}^n > 0$), then the numerical flux for $F_{j,i-\frac{1}{2}}^n$ is chosen as $u_{j,i-1}^n(-d_j \mathbf{P}_{i-\frac{1}{2}}^n)$; otherwise, we take $u_{j,i}^n(-d_j \mathbf{P}_{i-\frac{1}{2}}^n)$.

For simplicity, we set the notations:

$$G_i^{n-1} := u_{1,i}^{n-1} + u_{2,i}^{n-1}, \qquad E_{j,i}^n := u_{j,i}^n h_{j,\alpha_j}\left(u_{1,i}^{n-1}, u_{2,i}^{n-1}\right) \qquad (j = 1,2).$$

The time delay terms $h_{j,\alpha_j}(u_{1,i}^{n-1}, u_{2,i}^{n-1})(j = 1,2)$ are approximated by

$$h_{1,\alpha_1}\left(u_{1,i}^{n-1}, u_{2,i}^{n-1}\right) = b_1 - \delta_1 - \left(a_{11} u_{1,i}^{n-1-m_1} + a_{12} u_{2,i}^{n-1}\right),$$

$$h_{2,\alpha_2}\left(u_{1,i}^{n-1}, u_{2,i}^{n-1}\right) = b_2 - \delta_2 - \left(a_{21} u_{1,i}^{n-1} + a_{22} u_{2,i}^{n-1-m_2}\right),$$

where the integers $m_j (j = 1,2)$ satisfy

$$t_{n-1} - \alpha_j = \left(n - 1 - m_j\right)\tau.$$

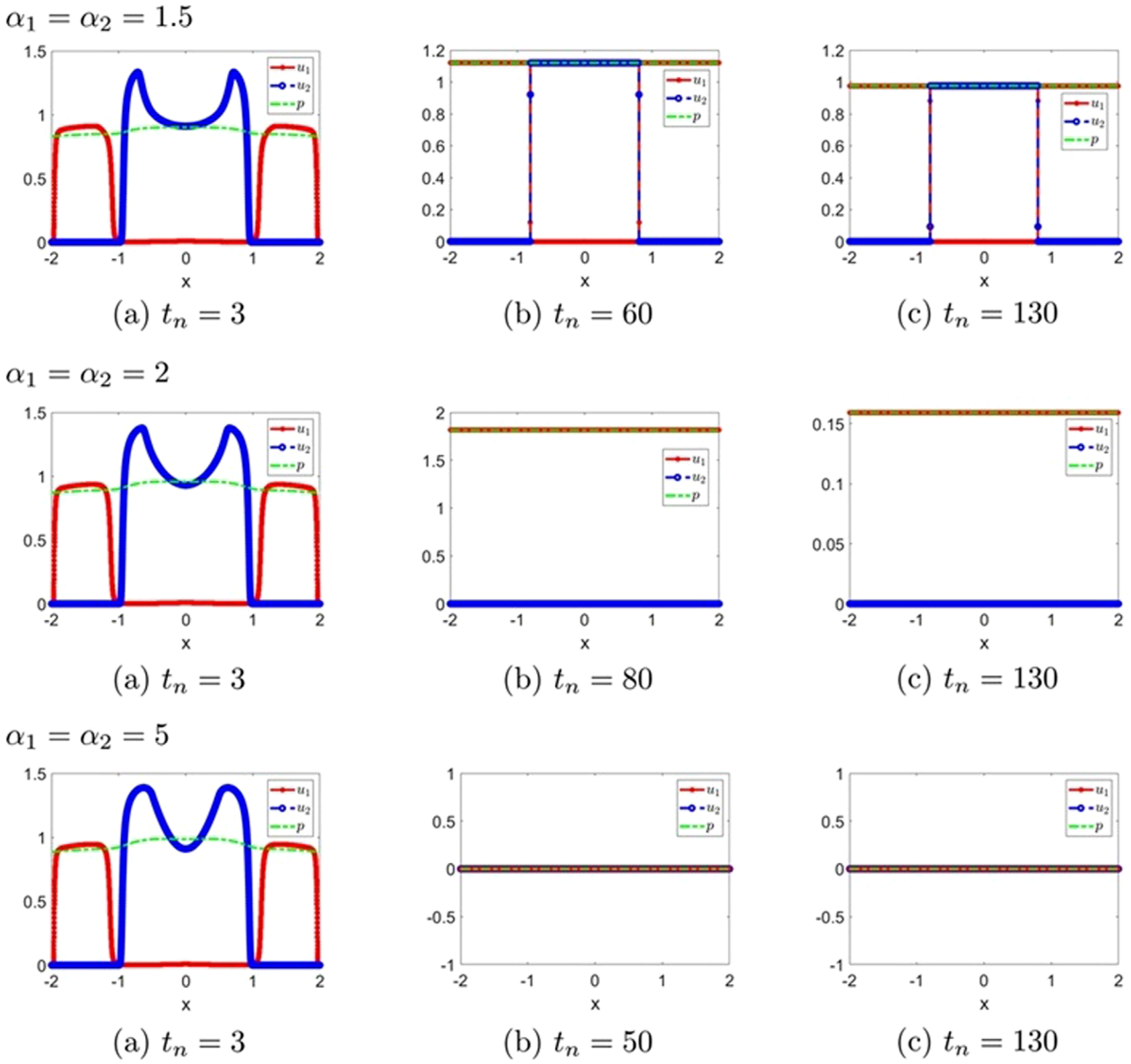

FIGURE 4
The numerical solution (Examples 1-2-3, 1-2-4, 1-2-5). **(a–c)** show the evaluation of the numerical solution at different times.

For $1 \le i \le N_c$, by the fact that $|C_i| = h_i$, we get the finite volume scheme (FVM) scheme.

$$p_i^n - \frac{\chi}{h_i}\left(\mathbf{P}^n_{i+\frac{1}{2}} - \mathbf{P}^n_{i-\frac{1}{2}}\right) = G_i^{n-1}, \tag{2.4a}$$

$$u_{1,i}^n + \frac{\tau}{h_i}\left(F^n_{1,i+\frac{1}{2}} - F^n_{1,i-\frac{1}{2}}\right) + \tau E^n_{1,i} = u_{1,i}^{n-1}, \tag{2.4b}$$

$$u_{2,i}^n + \frac{\tau}{h_i}\left(F^n_{2,i+\frac{1}{2}} - F^n_{2,i-\frac{1}{2}}\right) + \tau E^n_{2,i} = u_{2,i}^{n-1}. \tag{2.4c}$$

2.2.2 Positivity-preserving property

In this section, we show the positivity-preserving for the discrete solutions. We set $\boldsymbol{u}^n_{j,h} = (u^n_{j,1}, \ldots, u^n_{j,N_c})^\top$.

Theorem 2.1: *Assume that $\boldsymbol{u}^k_{j,h}$ $(k \le n-1,\ j = 1,2)$ are nonnegative and not identically zero. If τ is sufficiently small such that $\tau < \min\{\frac{1}{b_1-\delta_1}, \frac{1}{b_2-\delta_2}\}$, then we have:*

$$\boldsymbol{u}^n_{1,h} \ge 0, \quad \boldsymbol{u}^n_{2,h} \ge 0 \qquad (\forall n \ge 1).$$

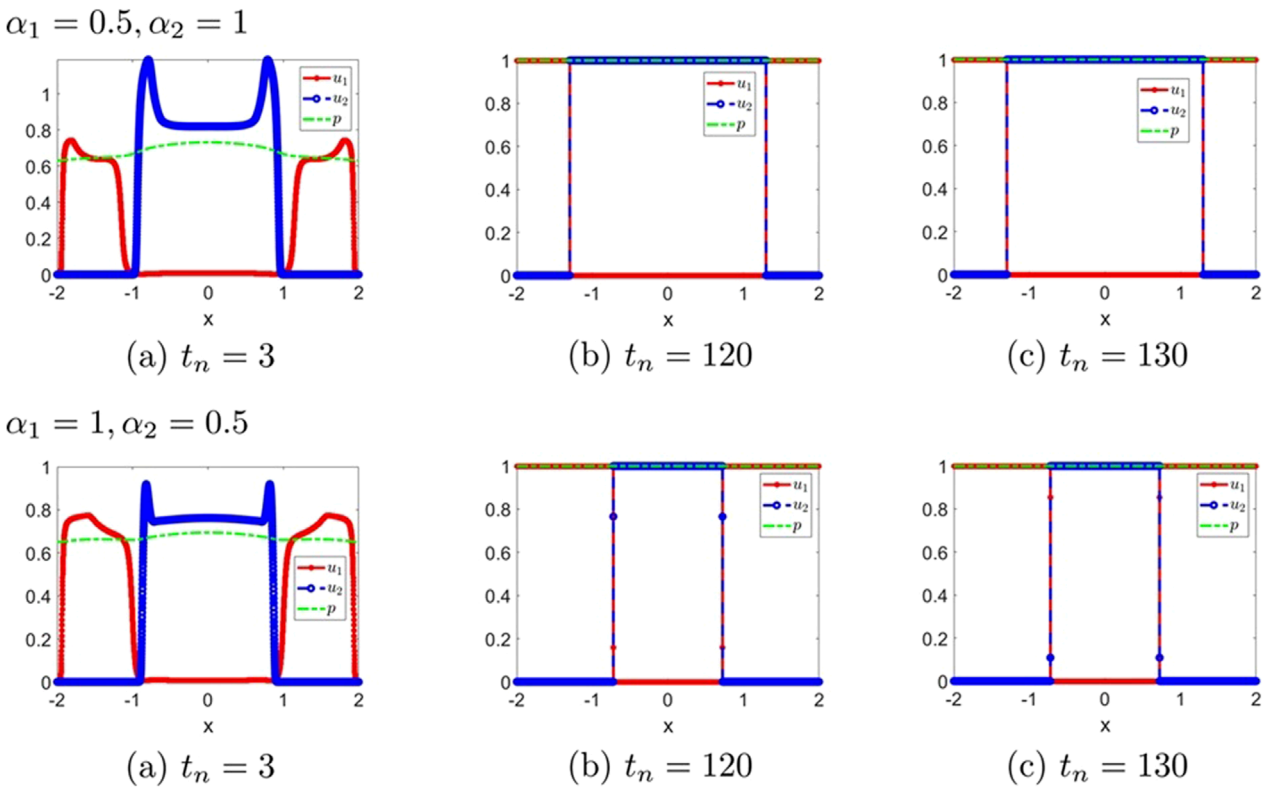

FIGURE 5
The numerical solution (Examples 1-2-6, 1-2-7). **(a–c)** show the evaluation of the numerical solution at different times.

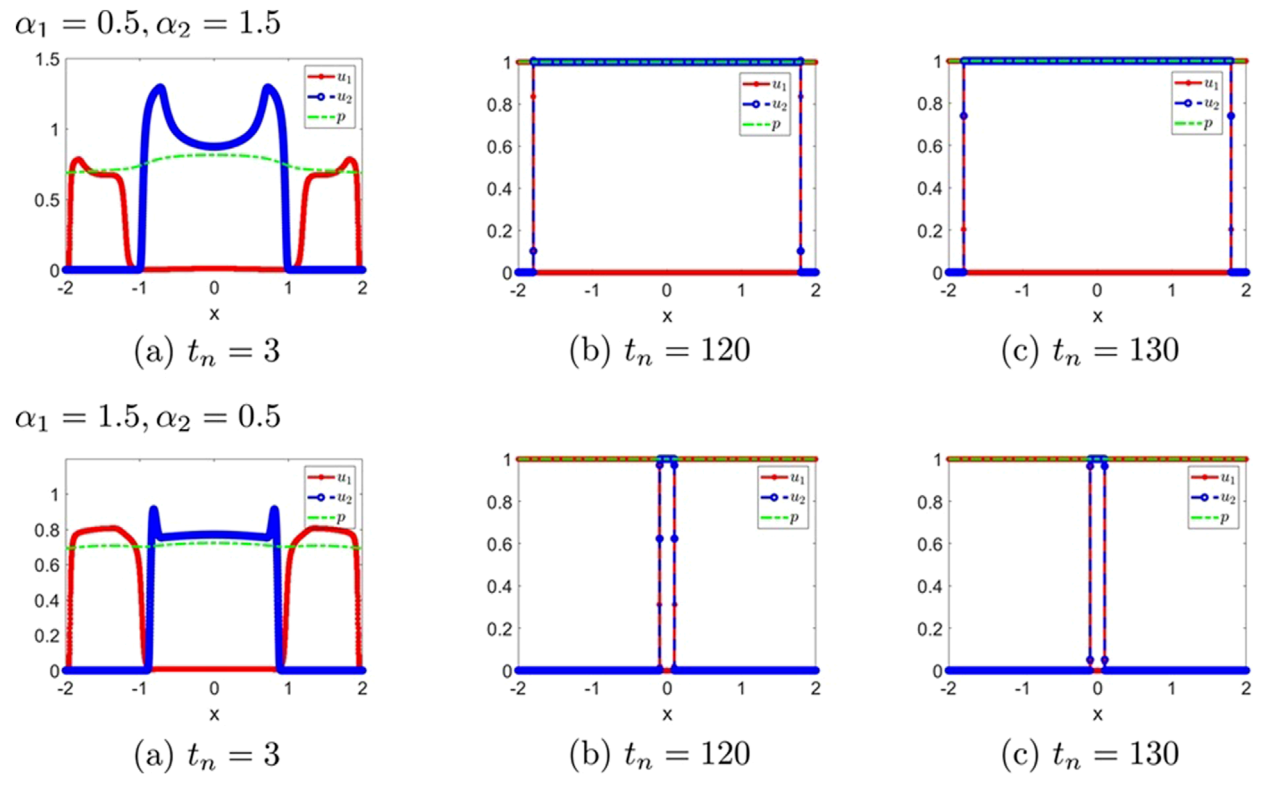

FIGURE 6
The numerical solution (Examples 1-2-8, 1-2-9). **(a–c)** show the evaluation of the numerical solution at different times.

TABLE 3 Classification of asymptotic behavior ($\alpha_1 = \alpha_2$).

Example	$\alpha_1 = \alpha_2$	Steady state	Long time behavior
Example 1-2-1	0.1	Steady state	Both non-vanishing and steady
Example 1-2-2	0.5	Steady state	Both non-vanishing and steady
Example 1-2-3	1.5	No steady state	Both non-vanishing and unsteady
Example 1-2-4	2	No steady state	One vanished and the other one is unsteady
Example 1-2-5	5	No steady state	Both vanished

TABLE 4 Classification of asymptotic behavior ($\alpha_1 \neq \alpha_2$).

Example	α_1	α_2	Long time behavior
Example 1-2-6	0.5	1	Steady and u_2 superior
Example 1-2-7	1	0.5	Steady and u_1 superior
Example 1-2-8	0.5	1.5	Steady and u_2 superior
Example 1-2-9	1.5	0.5	Steady and u_1 superior

Proof. The discrete system Equations 2.4b, 2.4c can be rewritten into the matrix forms:

$$\mathcal{A}_j^n \boldsymbol{u}_{j,h}^n = \boldsymbol{u}_{j,h}^{n-1} \qquad (j=1,2),$$

where $\mathcal{A}_j^n = (a_{j;i,s})_{1\le i,s\le N_c}$,

$$a_{j;i,s} = \begin{cases} 1 + \dfrac{\tau}{h_i}\left[-d_j \mathbf{P}^n_{i+\frac{1}{2}}\right]^+ + \dfrac{\tau}{h_i}\left[-d_j \mathbf{P}^n_{i-\frac{1}{2}}\right]^- - \tau h_{j,\alpha_j}\left(u_{1,i}^{n-1}, u_{2,i}^{n-1}\right) & s = i, \\ -\dfrac{\tau}{h_i}\left[-d_j \mathbf{P}^n_{i+\frac{1}{2}}\right]^- & s = i+1, \\ -\dfrac{\tau}{h_i}\left[-d_j \mathbf{P}^n_{i-\frac{1}{2}}\right]^+ & s = i-1, \\ 0 & \text{otherwise.} \end{cases}$$

We assume that $\boldsymbol{u}_{j,h}^k \ge 0, \neq 0$ $(k \le n-1,\ j=1,2)$. In view of Equations 2.2a, 2.2b, we see that $h_{j,\alpha_j}(u_{1,i}^{n-1}, u_{2,i}^{n-1}) \le b_j - \delta_j$ $(j=1,2)$. If we choose $\tau < \min\{\frac{1}{b_1-\delta_1}, \frac{1}{b_2-\delta_2}\}$, then we obtain:

$$1 - \tau h_{j,\alpha_j}\left(u_{1,i}^{n-1}, u_{2,i}^{n-1}\right) \ge 1 - \tau\left(b_j - \delta_j\right) > 0 \qquad (j=1,2).$$

The following statements hold for $\mathcal{A}_j^n$.

1. $\mathcal{A}_j^n$ has positive diagonal entries, i.e., for $j=1,2$ and $1 \le i \le N_c$,

$$1 + \frac{\tau}{h_i}\left[-d_j \mathbf{P}^n_{i+\frac{1}{2}}\right]^+ + \frac{\tau}{h_i}\left[-d_j \mathbf{P}^n_{i-\frac{1}{2}}\right]^- - \tau h_{j,\alpha_j}\left(u_{1,i}^{n-1}, u_{2,i}^{n-1}\right) > 0.$$

2. $\mathcal{A}_j^n$ has non-positive off-diagonal entries, i.e., for $j=1,2$ and $1 \le i \le N_c$,

$$-\frac{\tau}{h_i}\left[-d_j \mathbf{P}^n_{i+\frac{1}{2}}\right]^- \le 0, \qquad -\frac{\tau}{h_i}\left[-d_j \mathbf{P}^n_{i-\frac{1}{2}}\right]^+ \le 0.$$

3. All the column sums of $\mathcal{A}_j^n$ are positive, i.e., for $j=1,2$ and $1 \le i \le N_c$,

$$a_{j;i-1,i} + a_{j;i,i} + a_{j;i+1,i} = 1 - \tau h_{j,\alpha_j}\left(u_{1,i}^{n-1}, u_{2,i}^{n-1}\right) \ge 1 - \tau\left(b_j - \delta_j\right) > 0.$$

According to a convenient sufficient but not necessary condition of M-matrices (cf. [5, Appendix]), we conclude that $\mathcal{A}_j^n$ is an M-matrix.

According to the properties of M-matrices, this implies that $(\mathcal{A}_j^n)^{-1} > 0$ $(j=1,2)$. Noting that $\boldsymbol{u}_{j,h}^k \ge 0, \neq 0$ $(k \le n-1,\ j=1,2)$, we have $\boldsymbol{u}_{j,h}^n = (\mathcal{A}_j^n)^{-1}\boldsymbol{u}_{j,h}^{n-1} \ge 0$. By induction, we conclude that $\boldsymbol{u}_{j,h}^n \ge 0$ $(j=1,2)$ for all n.

2.2.3 The discrete conservation laws

The purpose of this section is to establish the mass conservation property of the (FVM) scheme (see Equations 2.4a–2.4c).

Theorem 2.2: *Let $u_{j,h}^n$ $(j=1,2)$ be the solution of (FVM). Then, we have the discrete conservation law:*

$$\sum_{i=1}^{N_c} u_{j,i}^n - \sum_{i=1}^{N_c} u_{j,i}^{n-1} = \sum_{i=1}^{N_c} \tau E_{j,i}^n \qquad (j=1,2).$$

Moreover, under the assumptions that $h_{j,\alpha_j} = 0$ $(j=1,2)$, it follows that

$$\sum_{i=1}^{N_c} u_{j,i}^n = \sum_{i=1}^{N_c} u_{j,i}^0 \qquad (j=1,2).$$

Proof. Summing up Equations 2.4b, 2.4c with respect to i, we obtain

$$\sum_{i=1}^{N_c} u_{j,i}^n + \sum_{i=1}^{N_c} \frac{\tau}{h_i}\left(F^n_{j,i+\frac{1}{2}} - F^n_{j,i-\frac{1}{2}}\right) + \sum_{i=1}^{N_c} \tau E_{j,i}^n = \sum_{i=1}^{N_c} u_{j,i}^{n-1} \qquad (j=1,2).$$

We see that

$$\sum_{i=1}^{N_c} \frac{\tau}{h_i}\left(F^n_{j,i+\frac{1}{2}} - F^n_{j,i-\frac{1}{2}}\right) = \frac{\tau}{h_i}\left(F^n_{j,N_c+\frac{1}{2}} - F^n_{j,\frac{1}{2}}\right) \qquad (j=1,2),$$

where

$$F^n_{j,\frac{1}{2}} = u^n_{j,0}\left[-d_j \mathbf{P}^n_{\frac{1}{2}}\right]^+ - u^n_{j,1}\left[-d_j \mathbf{P}^n_{\frac{1}{2}}\right]^- = 0$$

$$F^n_{j,N_c+\frac{1}{2}} = u^n_{j,N_c}\left[-d_j \mathbf{P}^n_{N_c+\frac{1}{2}}\right]^+ - u^n_{j,N_c+1}\left[-d_j \mathbf{P}^n_{N_c+\frac{1}{2}}\right]^- = 0$$

(by Equation 2.3).

Hence, we have

$$\sum_{i=1}^{N_c} u_{j,i}^n - \sum_{i=1}^{N_c} u_{j,i}^{n-1} = \sum_{i=1}^{N_c} \tau E_{j,i}^n \qquad (j=1,2).$$

TABLE 5 Experimental errors and convergence order of h for $\alpha_1 = \alpha_2 = 0$ (Example 2-1).

h	$\|u^N_{1,ref} - u^N_{1,h}\|_{L^2(I),\mathcal{V}_h}$	rate	$\|u^N_{2,ref} - u^N_{2,h}\|_{L^2(I),\mathcal{V}_h}$	rate	$\|p^N_{ref} - p^N_h\|_{H^1(I),\mathcal{V}_h}$	rate
1/80	6.10E-02	-	6.10E-02	-	2.24E-02	-
1/160	3.53E-02	0.79	3.56E-02	0.78	1.13E-02	0.99
1/320	1.95E-02	0.86	1.97E-02	0.85	5.37E-03	1.07
1/640	9.58E-03	1.02	9.70E-03	1.02	2.25E-03	1.26

TABLE 6 Experimental errors and convergence order of h for $\alpha_1 = \alpha_2 = 0.5$ (Example 2-2-2).

h	$\|u^N_{1,ref} - u^N_{1,h}\|_{L^2(I),\mathcal{V}_h}$	rate	$\|u^N_{2,ref} - u^N_{2,h}\|_{L^2(I),\mathcal{V}_h}$	rate	$\|p^N_{ref} - p^N_h\|_{H^1(I),\mathcal{V}_h}$	rate
1/80	6.14E-02	-	6.14E-02	-	2.28E-02	-
1/160	3.54E-02	0.79	3.58E-02	0.78	1.14E-02	1.00
1/320	1.94E-02	0.87	1.97E-02	0.86	5.40E-03	1.08
1/640	9.50E-03	1.04	9.60E-03	1.03	2.20E-03	1.27

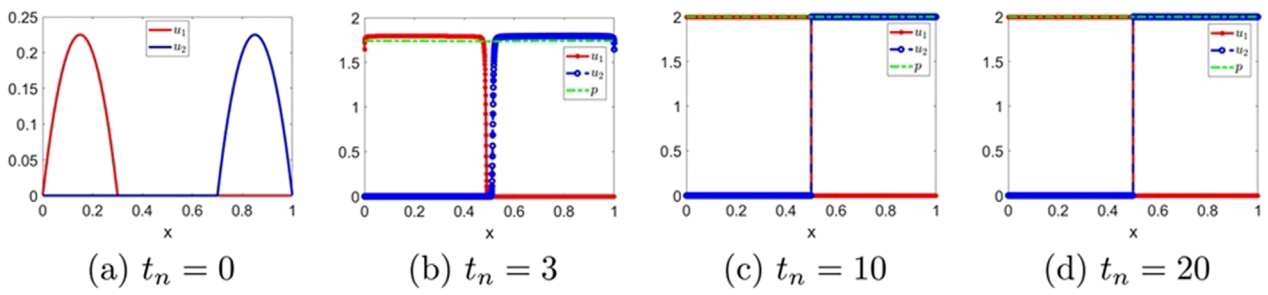

FIGURE 7
The numerical solution for $\alpha_1 = \alpha_2 = 0$ (Example 2-1). **(a–d)** show the evaluation of the numerical solution at different times.

Moreover, if we assume that $h_{j,\alpha_j} = 0$ (i.e., $E^n_{j,i} = 0$), then we have

$$\sum_{i=1}^{N_c} u^n_{j,i} = \sum_{i=1}^{N_c} u^{n-1}_{j,i} = \sum_{i=1}^{N_c} u^0_{j,i} \qquad (j = 1,2).$$

Hence the proof is complete.

Remark 2.3: For hyperbolic systems, there exist other positivity-preserving strategies, such as the linear scaling limiter [35, 36], which enforces bounds in finite volume and discontinuous Galerkin methods through constraints at Legendre Gauss-Lobatto points.

3 Numerical experiments

In this section, we conduct extensive numerical experiments, where we examine the numerical convergence orders, compare the results with the classical hyperbolic Keller–Segel system, and investigate the influence of time delays on competitive dynamics under various parameter settings. We take $\delta_j = 0$ $(j = 1,2)$ in this section. We set.

$$\|v\|_{L^2(I),\mathcal{V}_h} = \left(\sum_{i=1}^{N_c} |v(x_i)|^2 |C_i|\right)^{\frac{1}{2}} \forall v \in \mathcal{V}_h,$$

$$|v|_{H^1(I),\mathcal{V}_h} = \left(\sum_{i=1}^{N_c} \frac{|v(x_i) - v(x_{i-1})|^2}{|x_i - x_{i-1}|}\right)^{\frac{1}{2}} \forall v \in \mathcal{V}_h,$$

$$\|v\|_{H^1(I),\mathcal{V}_h} = \left(\|v\|^2_{L^2(I),\mathcal{V}_h} + |v|^2_{H^1(I),\mathcal{V}_h}\right)^{\frac{1}{2}} \forall v \in \mathcal{V}_h.$$

3.1 Example 1 (non-segregated initial functions)

We set $I = [-2,2]$, $\chi = 1$, $d_1 = 4$, $d_2 = 1$, and

$$h_{1,\alpha_1}((u_1,u_2)(t,x)) = 1 - u_1(t-\alpha_1,x) - 2u_2(t,x),$$
$$h_{2,\alpha_2}((u_1,u_2)(t,x)) = 1 - 2u_1(t,x) - u_2(t-\alpha_2,x).$$

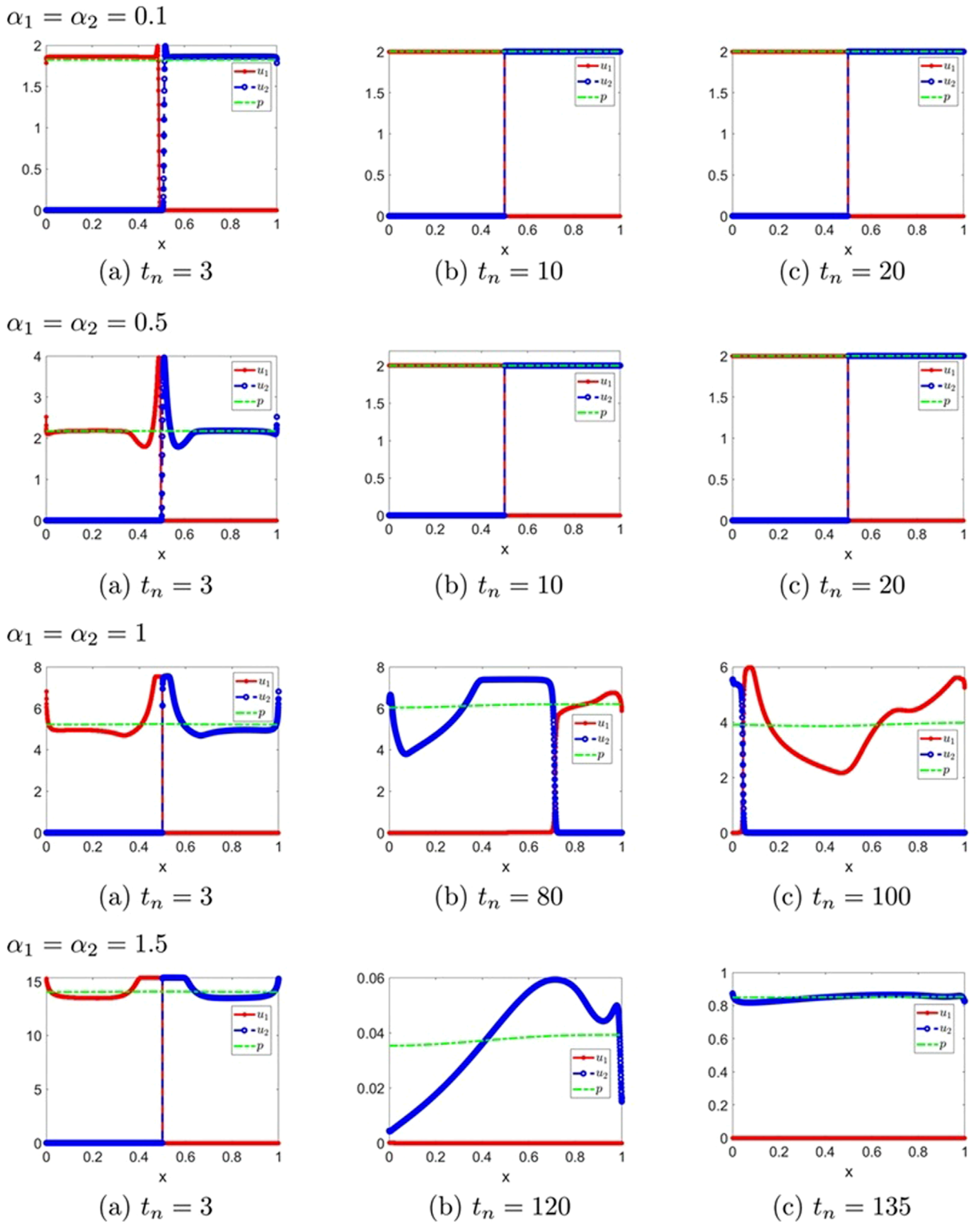

FIGURE 8
The numerical solution (Examples 2-2-1 through 2-2-4). **(a–c)** show the evaluation of the numerical solution at different times.

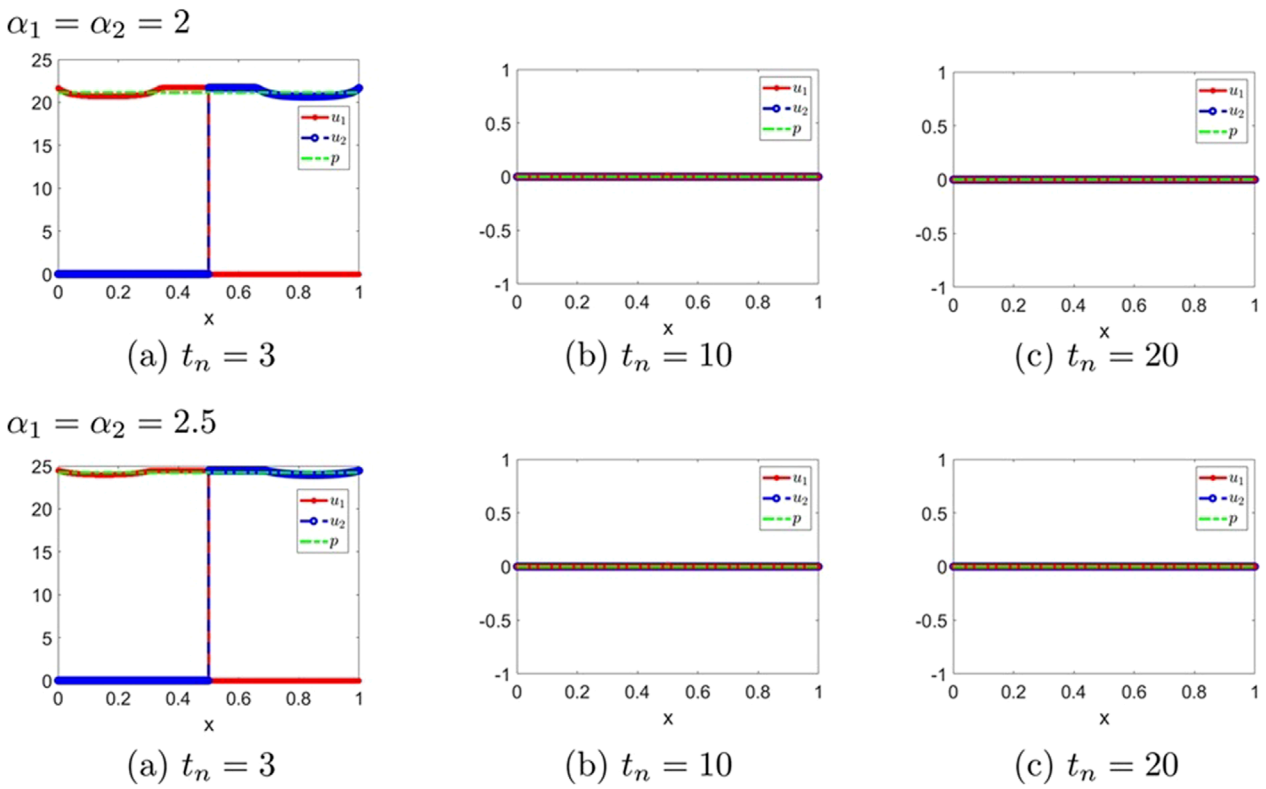

FIGURE 9
The numerical solution (Examples 2-2-5, 2-2-6). (**a–c**) show the evaluation of the numerical solution at different times.

The initial conditions are chosen as follows:

$$u_1(t,x) = \begin{cases} 0.25 - x^2 & -0.5 \le x \le 0.5 \\ 0 & \text{otherwise} \end{cases} \quad \text{for all } t \le 0,$$

$$u_2(t,x) = \begin{cases} 2\left(0.25 - x^2\right) & -0.5 \le x \le 0.5 \\ 0 & \text{otherwise} \end{cases} \quad \text{for all } t \le 0.$$

To examine the influence of time delays on competitive dynamics under varying parameter settings, the following cases are considered.

1. the classical hyperbolic Keller–Segel system
   - Example 1-1: $\alpha_1 = \alpha_2 = 0$;
2. $\alpha_1 = \alpha_2$
   - Example 1-2-1: $\alpha_1 = \alpha_2 = 0.1$;
   - Example 1-2-2: $\alpha_1 = \alpha_2 = 0.5$;
   - Example 1-2-3: $\alpha_1 = \alpha_2 = 1.5$;
   - Example 1-2-4: $\alpha_1 = \alpha_2 = 2$;
   - Example 1-2-5: $\alpha_1 = \alpha_2 = 5$;
3. $\alpha_1 \neq \alpha_2$
   - Example 1-2-6: $\alpha_1 = 0.5, \alpha_2 = 1$;
   - Example 1-2-7: $\alpha_1 = 1, \alpha_2 = 0.5$;
   - Example 1-2-8: $\alpha_1 = 0.5, \alpha_2 = 1.5$;
   - Example 1-2-9: $\alpha_1 = 1.5, \alpha_2 = 0.5$.

To obtain the experimental convergence order of the mesh size h, we fix $\tau = \frac{1}{2000}$, use the numerical solution with $h = \frac{1}{2000}$ at $T = 1$ as the reference solution (denoted by $(u^N_{1,ref}, u^N_{2,ref}, p^N_{ref})$), and compute the errors for different mesh sizes $h = \frac{1}{80}, \frac{1}{160}, \frac{1}{320}, \frac{1}{640}$. For the classical hyperbolic Keller–Segel system (i.e., $\alpha_1 = \alpha_2 = 0$), the experimental errors are shown in Table 1. For the system with time delay ($\alpha_1 = \alpha_2 = 0.5$), the experimental errors are presented in Table 2. We observe the first-order convergence with respect to the mesh size h for $\|u^N_{j,ref} - u^N_{j,h}\|_{L^2(I),\mathcal{V}_h}$ ($j = 1, 2$) and $\|p^N_{ref} - p^N_h\|_{H^1(I),\mathcal{V}_h}$.

The evolution of the solutions for the classical hyperbolic Keller–Segel system (i.e., $\alpha_1 = \alpha_2 = 0$) with $h = \tau = \frac{1}{1000}$ is shown in Figure 2. The solution dynamics of the time-delayed nonlocal advection model with $h = \tau = \frac{1}{1000}$ are presented in Figures 3–6. We classify the dynamic behaviors for $\alpha_1 = \alpha_2$ and $\alpha_1 \neq \alpha_2$ in Tables 3, 4, respectively. For the non-segregated initial function cases, small symmetric delays ($\alpha_1 = \alpha_2 \le 0.5$) lead to steady coexistence (see Example 1-2-1 – Example 1-2-2, Figure 3), while larger delays ($\alpha_1 = \alpha_2 \ge 1.5$) cause unsteady dynamics and potential extinction of one or both species (see Example 1-2-3 – Example 1-2-5, Figure 4). When the time delay is identical for both species (i.e., $\alpha_1 = \alpha_2$) and sufficiently large, the delayed competitive feedback leads to an unsteady system. The populations overreact to outdated density information, causing oscillations that eventually drive both species to extinction, as seen in the numerical results. For the case with asymmetric delays, we observe that the species with the larger delay is dominance in the competition (e.g., u_2 dominates when $\alpha_1 < \alpha_2$, or *vice versa* (see Example 1-2-6 – Example 1-2-9, Figures 5, 6)).

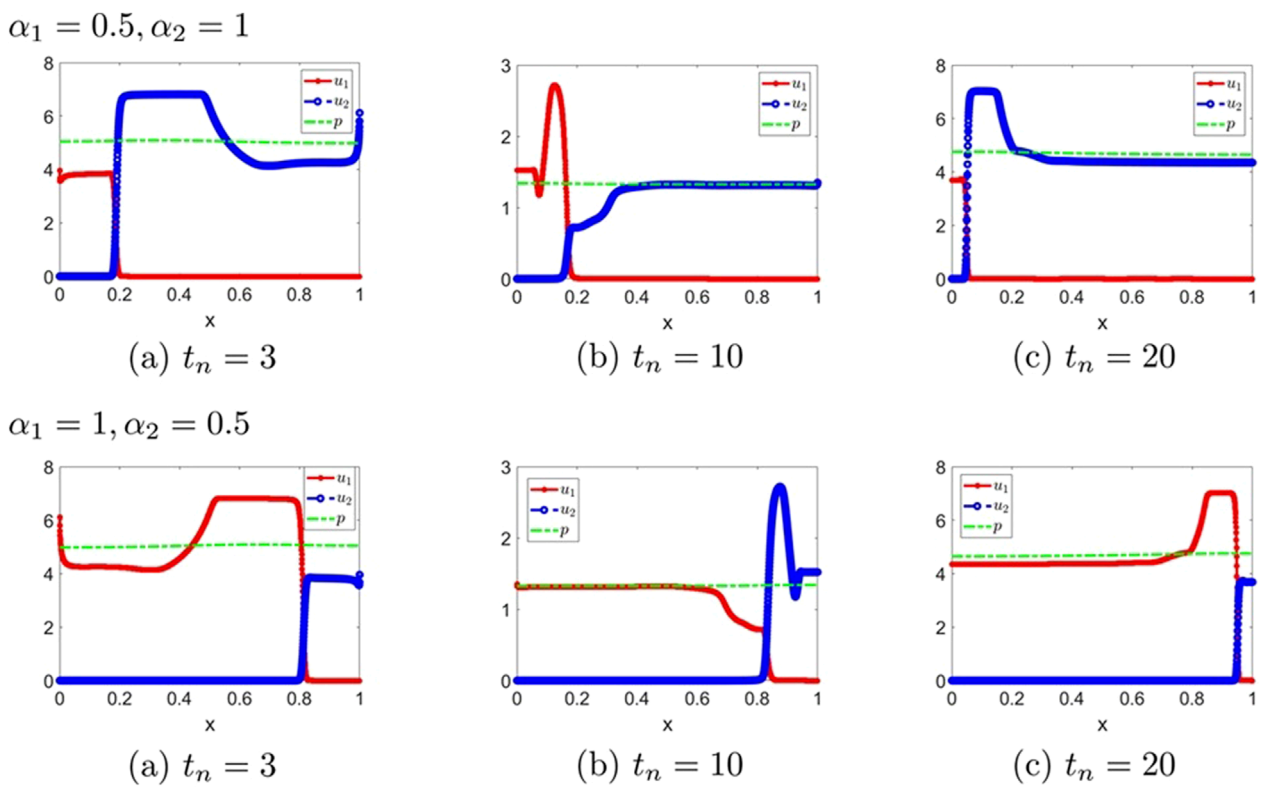

FIGURE 10
The numerical solution (Examples 2-2-7, 2-2-8). **(a–c)** show the evaluation of the numerical solution at different times.

TABLE 7 Classification of asymptotic behavior ($\alpha_1 = \alpha_2$).

Example	$\alpha_1 = \alpha_2$	Steady state	Long time behavior
Example 2-2-1	0.1	Steady state	Both non-vanishing and steady
Example 2-2-2	0.5	Steady state	Both non-vanishing and steady
Example 2-2-3	1	No steady state	Both non-vanishing and unsteady
Example 2-2-4	1.5	No steady state	One vanished and the other one is unsteady
Example 2-2-5	2	No steady state	Both vanished
Example 2-2-6	2.5	No steady state	Both vanished

TABLE 8 Classification of asymptotic behavior ($\alpha_1 \neq \alpha_2$).

Example	α_1	α_2	Long time behavior
Example 2-2-7	0.5	1	Unsteady and u_2 superior
Example 2-2-8	1	0.5	Unsteady and u_1 superior

3.2 Example 2 (segregated initial functions)

Set $I = [0,1]$, $\chi = 1$, $d_1 = 1$, $d_2 = 1$, and

$$h_{1,\alpha_1}((u_1,u_2)(t,x)) = 2 - u_1(t-\alpha_1,x) - u_2(t,x),$$
$$h_{2,\alpha_2}((u_1,u_2)(t,x)) = 2 - u_1(t,x) - u_2(t-\alpha_2,x).$$

TABLE 9 Experimental errors and convergence order of h for $\alpha_1 = \alpha_2 = 0$ (Example 3-1).

h	$\|u^N_{1,ref} - u^N_{1,h}\|_{L^2(I),\mathcal{V}_h}$	rate	$\|u^N_{2,ref} - u^N_{2,h}\|_{L^2(I),\mathcal{V}_h}$	rate	$\|p^N_{ref} - p^N_h\|_{H^1(I),\mathcal{V}_h}$	rate
1/80	6.28E-02	-	6.25E-02	-	2.12E-02	-
1/160	3.61E-02	0.80	3.69E-02	0.76	1.07E-02	0.99
1/320	1.99E-02	0.86	2.05E-02	0.84	5.12E-03	1.07
1/640	9.77E-03	1.03	1.02E-02	1.01	2.15E-03	1.25

TABLE 10 Experimental errors and convergence order of h for $\alpha_1 = \alpha_2 = 0.5$ (Example 3-2-2).

h	$\|u^N_{1,ref} - u^N_{1,h}\|_{L^2(I),\mathcal{V}_h}$	rate	$\|u^N_{2,ref} - u^N_{2,h}\|_{L^2(I),\mathcal{V}_h}$	rate	$\|p^N_{ref} - p^N_h\|_{H^1(I),\mathcal{V}_h}$	rate
1/80	6.46E-02	-	6.27E-02	-	2.20E-02	-
1/160	3.71E-02	0.80	3.68E-02	0.77	1.10E-02	0.99
1/320	2.04E-02	0.86	2.03E-02	0.86	5.20E-03	1.08
1/640	1.01E-02	1.02	1.00E-02	1.03	2.20E-03	1.27

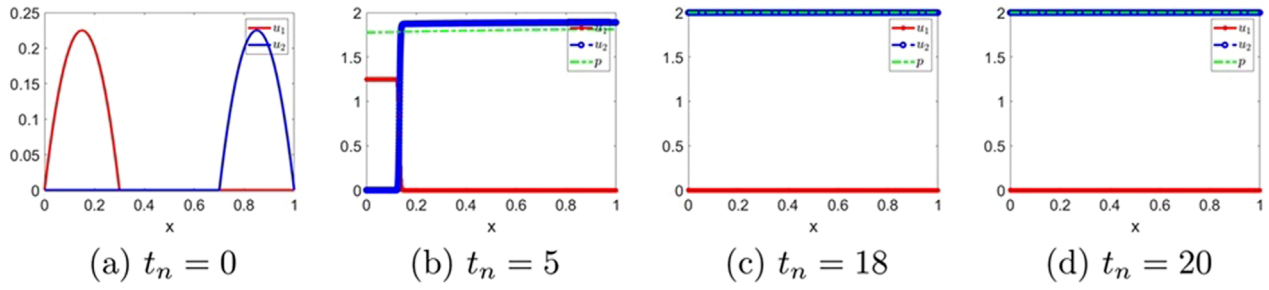

FIGURE 11
The numerical solution for $\alpha_1 = \alpha_2 = 0$ (Example 3-1). **(a–d)** show the evaluation of the numerical solution at different times.

The initial conditions are set to

$$u_1(t,x) = \begin{cases} -10x(x-0.3) & 0 \le x \le 0.3 \\ 0 & \text{otherwise} \end{cases} \quad \text{for all } t \le 0,$$

$$u_2(t,x) = \begin{cases} -10(1-x)(0.7-x) & 0.7 \le x \le 1 \\ 0 & \text{otherwise} \end{cases} \quad \text{for all } t \le 0.$$

We consider the following settings.

1. the classical hyperbolic Keller–Segel system
   - Example 2-1: $\alpha_1 = \alpha_2 = 0$;
2. $\alpha_1 = \alpha_2$
   - Example 2-2-1: $\alpha_1 = \alpha_2 = 0.1$,
   - Example 2-2-2: $\alpha_1 = \alpha_2 = 0.5$,
   - Example 2-2-3: $\alpha_1 = \alpha_2 = 1$,
   - Example 2-2-4: $\alpha_1 = \alpha_2 = 1.5$,
   - Example 2-2-5: $\alpha_1 = \alpha_2 = 2$,
   - Example 2-2-6: $\alpha_1 = \alpha_2 = 2.5$;
3. $\alpha_1 \neq \alpha_2$
   - Example 2-2-7: $\alpha_1 = 0.5, \alpha_2 = 1$,
   - Example 2-2-8: $\alpha_1 = 1, \alpha_2 = 0.5$.

We fix $\tau = \frac{1}{2000}$, take the numerical solution with $h = \frac{1}{2000}$ at $T = 1$ as the reference solution, and compute the errors for mesh sizes $h = \frac{1}{80}, \frac{1}{160}, \frac{1}{320}, \frac{1}{640}$. The experimental errors for $\alpha_1 = \alpha_2 = 0$ and $\alpha_1 = \alpha_2 = 0.5$, shown in Tables 5, 6, respectively, indicate first-order convergence with respect to the mesh size h for $\|u^N_{j,ref} - u^N_{j,h}\|_{L^2(I),\mathcal{V}_h}$ $(j = 1, 2)$ and $\|p^N_{ref} - p^N_h\|_{H^1(I),\mathcal{V}_h}$.

Figure 7 displays the evolution of solutions for the classical Keller–Segel system with $h = \tau = \frac{1}{2000}$. Figures 8–10 illustrate the dynamic behavior of the time-delayed nonlocal advection model with $h = \tau = \frac{1}{1000}$. Tables 7, 8 summarize the dynamic behaviors corresponding to the cases $\alpha_1 = \alpha_2$ and $\alpha_1 \neq \alpha_2$, respectively. Symmetric delays in segregated initial functions, where the coefficients for h_{1,α_1} and h_{2,α_2} are the same, demonstrate that small delays $(\alpha_1 = \alpha_2 \le 0.5)$ can support steady coexistence. However, larger delays $(\alpha_1 = \alpha_2 \ge 1)$ may result in unsteady states or extinction. In Figure 10, we consider the case where $\alpha_1 \neq \alpha_2$, revealing that the species with the larger delay often gain a competitive advantage.

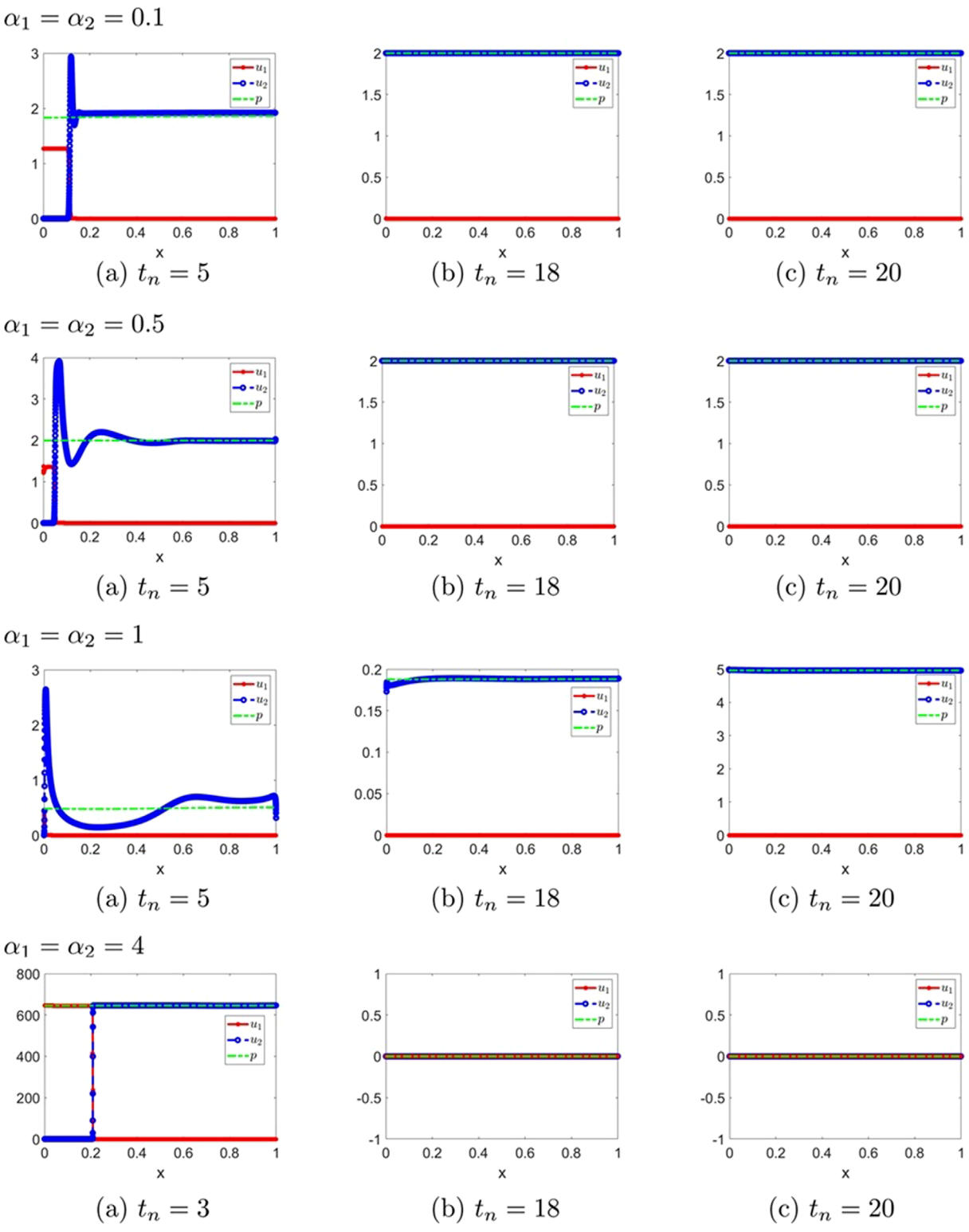

FIGURE 12
The numerical solution (Examples 3-2-1 through 3-2-4). **(a–c)** show the evaluation of the numerical solution at different times.

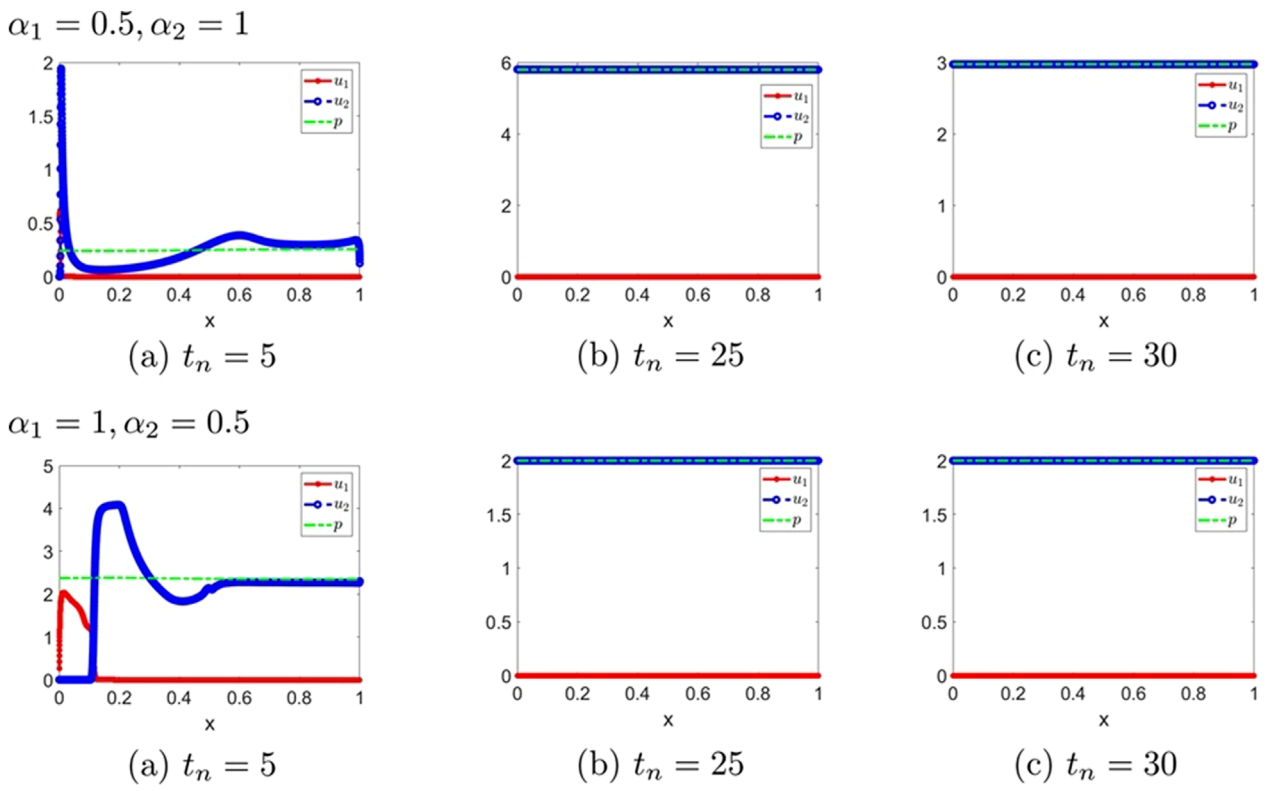

FIGURE 13
The numerical solution (Examples 3-2-5, 3-2-6). **(a–c)** show the evaluation of the numerical solution at different times.

TABLE 11 Classification of asymptotic behavior ($\alpha_1 = \alpha_2$).

Example	$\alpha_1 = \alpha_2$	Steady state	Long time behavior
Example 3-2-1	0.1	Steady state	One vanished and the other one is steady
Example 3-2-2	0.5	Steady state	One vanished and the other one is steady
Example 3-2-3	1	No steady state	One vanished and the other one is unsteady
Example 2-2-4	4	No steady state	Both vanished

3.3 Example 3 (segregated initial functions)

The settings are the same as those in Example 2, except that we choose

$$h_{1,\alpha_1}((u_1,u_2)(t,x)) = 2 - 2u_1(t-\alpha_1,x) - 2u_2(t,x),$$
$$h_{2,\alpha_2}((u_1,u_2)(t,x)) = 2 - u_1(t,x) - u_2(t-\alpha_2,x).$$

The following parameters are considered.

1. the classical hyperbolic Keller–Segel system
   - Example 3-1: $\alpha_1 = \alpha_2 = 0$;
2. $\alpha_1 = \alpha_2$
   - Example 3-2-1: $\alpha_1 = \alpha_2 = 0.1$,
   - Example 3-2-2: $\alpha_1 = \alpha_2 = 0.5$,
   - Example 3-2-3: $\alpha_1 = \alpha_2 = 1$,
   - Example 3-2-4: $\alpha_1 = \alpha_2 = 4$;
3. $\alpha_1 \neq \alpha_2$
   - Example 3-2-5: $\alpha_1 = 0.5, \alpha_2 = 1$,
   - Example 3-2-6: $\alpha_1 = 1, \alpha_2 = 0.5$.

We fix $\tau = \frac{1}{2000}$, take the numerical solution with $h = \frac{1}{2000}$ at $T = 1$ as the reference solution, and compute the errors for mesh sizes $h = \frac{1}{80}, \frac{1}{160}, \frac{1}{320}, \frac{1}{640}$. First-order convergence with respect to the mesh size h is observed for $\|u^N_{j,ref} - u^N_{j,h}\|_{L^2(I),\mathcal{V}_h}$ $(j = 1,2)$ and $\|p^N_{ref} - p^N_h\|_{H^1(I),\mathcal{V}_h}$, as shown in Table 9 for $\alpha_1 = \alpha_2 = 0$, and Table 10 for $\alpha_1 = \alpha_2 = 0.5$.

The evolutions of the solution for the classical Keller–Segel system ($h = \tau = \frac{1}{5000}$) are shown in Figure 11. Figures 12, 13 present the evolutions of the solution for the nonlocal advection model with time delays ($h = \tau = \frac{1}{5000}$). The dynamic behaviors for $\alpha_1 =$

TABLE 12 Classification of asymptotic behavior ($\alpha_1 \neq \alpha_2$).

Example	α_1	α_2	Long time behavior
Example 3-2-5	0.5	1	Unsteady and u_2 superior
Example 3-2-6	1	0.5	Steady and u_2 superior

α_2 and $\alpha_1 \neq \alpha_2$ are summarized in Tables 11, 12, respectively. For the symmetric delays in the segregated initial functions, where the coefficients for h_{1,α_1} and h_{2,α_2} differ, small delays ($\alpha_1 = \alpha_2 \leq 0.5$) still result in the steady state (see Example 3-2-1 – Example 3-2-2, Figure 12). On the other hand, larger delays ($\alpha_1 = \alpha_2 \geq 1$) can lead to unsteady dynamics and extinction (see Example 3-2-3 – Example 3-2-4, Figure 12). For the case with asymmetric delays, we see that both two examples are u_2 superior (see Example 3-2-5 – Example 3-2-6, Figure 13).

Remark 3.1: We observe that small symmetric delays ($\alpha_1 = \alpha_2$) result in the steady state. This suggests that ecosystems with balanced feedback mechanisms (e.g., similar resource recovery times for competing species) are more likely to maintain biodiversity. On the other hand, larger symmetric delays ($\alpha_1 = \alpha_2$) can lead to unsteady dynamics and extinction, which align with scenarios where delayed interventions (e.g., pesticide application or vaccination campaigns) fail to prevent population collapse. Moreover, asymmetric delay parameters ($\alpha_1 \neq \alpha_2$) between the two species tend to confer a competitive advantage to one species. Such dynamics are relevant in tumor-microenvironment interactions, where targeting delay mechanisms could alter competitive outcomes.

4 Conclusion

This study proposes a nonlocal advection model with time delays to investigate the population dynamics of two competing species, extending previous frameworks by incorporating delayed interactions between migration and resource recovery. A positivity-preserving finite volume scheme is developed to ensure biologically realistic solutions. Numerical experiments demonstrate that small symmetric delays ($\alpha_1 = \alpha_2$) are steady, while larger delays induce unsteady states and potential extinction of one or both species. Moreover, asymmetric delay parameters between the two species tend to confer a competitive advantage to one species. Future work may explore applications to more complex ecological systems, incorporate stochastic or spatially heterogeneous delays, and extend the model to multi-species interactions or adaptive delay mechanisms for deeper insights into delayed feedback effects in biological processes. As a future work, we would like to consider the development of high-dimensional chemotaxis models with time delays, explore alternative numerical schemes to improve computational efficiency, and ensure that the system properties (such as positivity preservation, conservation laws, and energy dissipation) are maintained.

Data availability statement

The original contributions presented in the study are included in the article/supplementary material, further inquiries can be directed to the corresponding author.

Author contributions

PZ: Writing – original draft, Data curation, Writing – review and editing, Methodology. YE: Writing – review and editing, Funding acquisition, Supervision, Methodology. GZ: Funding acquisition, Methodology, Supervision, Investigation, Writing – review and editing.

Funding

The author(s) declare that financial support was received for the research and/or publication of this article. This work was supported by JSPS KAKENHI Grant Number 25K07137, NSFC General Project No. 12171071, and the Natural Science Foundation of Sichuan Province No. 2023NSFSC0055.

Conflict of interest

The authors declare that the research was conducted in the absence of any commercial or financial relationships that could be construed as a potential conflict of interest.

Generative AI statement

The author(s) declare that no Generative AI was used in the creation of this manuscript.

Any alternative text (alt text) provided alongside figures in this article has been generated by Frontiers with the support of artificial intelligence and reasonable efforts have been made to ensure accuracy, including review by the authors wherever possible. If you identify any issues, please contact us.

Publisher's note

References

1. Murray JD. *Spatial models and biomedical applications*. New York: Springer (2003).

2. Murray JD. *Mathematical biology I. An introduction*, 17. Berlin: Springer (2007).

3. Pasquier J, Galas L, Boulangé-Lecomte C, Rioult D, Bultelle F, Magal P. Different modalities of intercellular membrane exchanges mediate cell-to-cell p-glycoprotein transfers in MCF-7 breast cancer cells. *J Biol Chem* (2012) 287(10):7374–87. doi:10.1074/jbc.M111.312157

4. Lou Y, Ni W. Diffusion, self-diffusion and cross-diffusion. *J Differ Equ* (1996) 131(1):79–131. doi:10.1006/jdeq.1996.0157

5. Lou Y, Ni W. Diffusion vs cross-diffusion: an elliptic approach. *J Differ Equ* (1999) 154(1):157–90. doi:10.1006/jdeq.1998.3559

6. Shigesada N, Kawasaki K, Teramoto E. Spatial segregation of interacting species. *J Theor Biol* (1979) 79(1):83–99. doi:10.1016/0022-5193(79)90258-3

7. Fu X, Griette Q, Magal P. A cell-cell repulsion model on a hyperbolic Keller–Segel equation. *J Math Biol* (2020) 80(7):2257–300. doi:10.1007/s00285-020-01495-w

8. Fu X, Magal P. Asymptotic behavior of a nonlocal advection system with two populations. *J Dyn Differ Equ* (2022) 34(3):2035–77. doi:10.1007/s10884-021-09956-6

9. Horstmann D. From 1970 until present: the Keller–Segel model in chemotaxis and its consequences. *Jahresber Dtsch Math.-Ver* (2003) 195(1):103–65. Available online at: https://cir.nii.ac.jp/crid/1571698600200464128

10. Horstmann D. From 1970 until present: the Keller–Segel model in chemotaxis and its consequences. *Jahresber Dtsch Math.-Ver* (2004) 106:51–69. Available online at: https://cir.nii.ac.jp/crid/1570291226041248512

11. Keller EF, Segel LA. Model for chemotaxis. *J Theor Biol* (1971) 30(2):225–34. doi:10.1016/0022-5193(71)90050-6

12. Patlak CS. Random walk with persistence and external bias. *Bull Math Biophys* (1953) 15:311–38. doi:10.1007/bf02476407

13. Fu X, Griette Q, Magal P. *Existence and uniqueness of solutions for a hyperbolic Keller–Segel equation*, Discrete Contin. *Dyn Syst Ser B* (2021) 26(4):1931–66. doi:10.3934/dcdsb.2020326

14. Perthame B, Dalibard A. Existence of solutions of the hyperbolic Keller–Segel model. *Trans Am Math Soc* (2009) 361(5):2319–35. doi:10.1090/s0002-9947-08-04656-4

15. Bruno L, Tosin A, Tricerri P, Venuti F. Non-local first-order modelling of crowd dynamics: a multidimensional framework with applications. *Appl Math Model* (2011) 35(1):426–45. doi:10.1016/j.apm.2010.07.007

16. Colombo RM, Garavello M, Lécureux-Mercier M. A class of nonlocal models for pedestrian traffic. *Math Models Methods Appl Sci* (2012) 22(4):1150023. doi:10.1142/s0218202511500230

17. Bürger R, Goatin P, Inzunza D, Villada LM. A non-local pedestrian flow model accounting for anisotropic interactions and domain boundaries. *Math Biosci Eng* (2020) 17(5):5883–906. doi:10.3934/mbe.2020314

18. Goatin P, Inzunza D, Villada LM. *Numerical comparison of nonlocal macroscopic models of multi-population pedestrian flows with anisotropic kernel*. Springer (2022). p. 371–81.

19. Kuang Y. *Delay differential equations*. New York: Academic Press (1993).

20. Smith HL. *An introduction to delay differential equations with applications to the life sciences*. New York: Springer (2011).

21. Volterra V. *Leçons sur la Théorie Mathématique de la Lutte pour la Vie*. Paris: Gauthier-Villars (1931).

22. Cushing JM. Time delays in single species growth models. *J Math Biol* (1977) 4(3):257–64. doi:10.1007/bf00280975

23. Cushing JM. Integrodifferential equations and delay models in population dynamics, 20. Berlin: Springer (2013).

24. Miller RK. On Volterra's population equation. *SIAM J Appl Math* (1966) 14(3):446–52. doi:10.1137/0114039

25. Bownds JM, Cushing JM. On the behavior of solutions of predator-prey equations with hereditary terms. *Math Biosci* (1975) 26(1-2):41–54. doi:10.1016/0025-5564(75)90093-0

26. Macdonald N. Time delay in prey-predator models. *Math Biosci* (1976) 28(3-4):321–30. doi:10.1016/0025-5564(76)90130-9

27. Gopalsamy K, Aggarwala BD. Limit cycles in two spacies competition with time delays. *J Austral Math Soc* (1980) 22(2):148–60. doi:10.1017/s033427000000223x

28. Shibata A, Saitô N. Time delays and chaos in two competing species. *Math Biosci* (1980) 51(3-4):199–211. doi:10.1016/0025-5564(80)90099-1

29. Saito N. Conservative upwind finite-element method for a simplified Keller–Segel system modelling chemotaxis. *IMA J Numer Anal* (2007) 27(2):332–65. doi:10.1093/imanum/drl018

30. Saito N. Error analysis of a conservative finite-element approximation for the Keller–Segel system of chemotaxis. *Commun Pure Appl Anal* (2011) 11(1):339–64. doi:10.3934/cpaa.2012.11.339

31. Saito N, Suzuki T. A finite difference scheme to the system of self-interacting particles. *RIMS Kôkyûroku* (2003) 1320:18–28. Available online at: http://hdl.handle.net/2433/43075

32. Saito N, Suzuki T. Notes on finite difference schemes to a parabolic-elliptic system modelling chemotaxis. *Appl Math Comput* (2005) 171(1):72–90. doi:10.1016/j.amc.2005.01.037

33. Zhou G, Saito N. Finite volume methods for a Keller–Segel system: discrete energy, error estimates and numerical blow-up analysis. *Numer Math* (2017) 135(1):265–311. doi:10.1007/s00211-016-0793-2

34. Cross L, Zhang X. *On the monotonicity of Q^2 spectral element method for Laplacian on quasi-uniform rectangular meshes*. *Commun Comput Phys* (2024) 35(1):60–180. doi:10.4208/cicp.oa-2023-0206

35. Zhang X, Shu C. On maximum-principle-satisfying high order schemes for scalar conservation laws. *J Comput Phys* (2010) 229(9):3091–120. doi:10.1016/j.jcp.2009.12.030

36. Zhang X, Shu C. Maximum-principle-satisfying and positivity-preserving high-order schemes for conservation laws: survey and new developments. *P Roy Soc A.-math Phy* (2011) 467(2134):2752–76. doi:10.1098/rspa.2011.0153